Dioxygen Activation

International Edition: DOI: 10.1002/anie.201510741
German Edition: DOI: 10.1002/ange.201510741

Quercetin 2,4-Dioxygenase Activates Dioxygen in a Side-On O_2–Ni Complex

*Jae-Hun Jeoung, Dimitrios Nianios, Susanne Fetzner, and Holger Dobbek**

Abstract: *Quercetin 2,4-dioxygenase (quercetinase) from Streptomyces uses nickel as the active-site cofactor to catalyze oxidative cleavage of the flavonol quercetin. How this unusual active-site metal supports catalysis and O_2 activation is under debate. We present crystal structures of Ni-quercetinase in three different states, thus providing direct insight into how quercetin and O_2 are activated at the Ni^{2+} ion. The Ni^{2+} ion is coordinated by three histidine residues and a glutamate residue (E^{76}) in all three states. Upon binding, quercetin replaces one water ligand at Ni and is stabilized by a short hydrogen bond through E^{76}, the carboxylate group of which rotates by 90°. This conformational change weakens the interaction between Ni and the remaining water ligand, thereby preparing a coordination site at Ni to bind O_2. O_2 binds side-on to the Ni^{2+} ion and is perpendicular to the C2–C3 and C3–C4 bonds of quercetin, which are cleaved in the following reaction steps.*

Decomposing plant material and exudates of roots and leaves liberate quercetin (3,5,7,3′,4′-pentahydroxyflavone, QUE) and other flavonoids,[1] which are catabolized or detoxified by soil microorganisms, filamentous fungi, and bacteria.[2] Aerobic microbial degradation of QUE is initiated by the 2,4-dioxygenolytic cleavage of QUE to generate 2-protocatechuoylphloroglucinol carboxylic acid (a depside) and carbon monoxide in a process catalysed by quercetin 2,4-dioxygenases (quercetinase, QueD).

QueDs belong to the cupin superfamily, members of which share a characteristic β-barrel fold. A conserved 3-His-1-Glu motif is used by QueDs to bind a metal ion, which is essential for their function.[3] While fungal QueD depends on Cu, bacterial QueDs show different levels of activity depending on the type of promiscuously bound metal. The structures of QueDs from *Aspergillus japonicus* ($QueD^{Aj}$) and *Bacillus subtilis* ($QueD^{Bs}$) were determined in the presence and absence of QUE and inhibitors.[4] However, how QueDs activate dioxygen is still under debate: either dioxygen reacts directly with QUE, and the metal ion just stabilizes the more reactive anionic form of QUE, or dioxygen is activated by binding to the active-site metal ion.[3,5] Mechanisms without direct binding of dioxygen to nickel are appealing for several reasons: QUE can react spontaneously with O_2, thus making O_2 activation at a metal site dispensable;[6] inorganic model catalysts that catalyze the breakdown of QUE with O_2 require no open coordination site at the metal;[7] cofactor-independent dioxygenases[8] can cleave heteroaromatic rings with dioxygen in the absence of metal ions; and the presence of different metal ions in the various QueDs suggests that the individual properties of the metals are not essential for catalysis.[3]

We investigated QueD from *Streptomyces* sp. strain FLA ($QueD^{FLA}$), which differs from the structurally characterized bicupin QueDs by its monocupin fold and type of active-site metal.[9] $QueD^{FLA}$ shows highest activity with Ni^{2+}, an unusual cofactor for oxygenases, but other divalent d-block metals, such as Co^{2+}, Mn^{2+}, and Fe^{2+} can replace Ni^{2+}, albeit with poorer (Co^{2+}, Mn^{2+}) or no (Fe^{2+}) catalytic activity.[9,10]

The purpose of our study was to define the catalytic role of nickel in QueDs. By using a crystallographic cryotrapping approach, we were able to show how binding of QUE primes Ni^{2+} to bind dioxygen side-on, ready to react with QUE.

We solved the crystal structure of $QueD^{FLA}$ by Ni-SAD phasing and refined the structures of three different states at resolutions of 1.8 to 2.15 Å (Table S1 in the Supporting Information). QueD is dimeric in solution[9a] and is found as a tightly packed homodimer in the asymmetric unit (ASU) of the crystal (Figure 1a). Each monomer forms the typical monocupin β-barrel fold and secures a nickel ion in the active site (one nickel per 180 residues). The N-terminal β-strand of the β-barrel originates from one monomer, while the remaining eleven β-strands are contributed by the other monomer. The two monomers are very similar and can be superimposed with a root-mean-square deviation (rmsd) of 0.4 Å for the Cα atoms. The Ni-$QueD^{FLA}$ dimer, assembled from two monocupins, is nearly identical to the domain arrangement found in the bicupin Cu- and Fe-containing QueDs, with an rmsd of 1.6–1.8 Å for the C_α atoms (Figure S5A).[4,5b]

The resting-state structure (free E) was refined at 1.8 Å resolution (Table S1). The nickel ion is coordinated by the Nε2 atoms of three His residues (H^{69}, H^{71}, and H^{115}), by Oε1 of E^{76} in a *syn*-monodentate manner, and by two water molecules (W1 and W2), to give an overall distorted octahedral arrangement (Figure 1b). Nickel–ligand bond lengths are 2.1–2.2 Å, as frequently observed in Ni complexes.[11] The second oxygen atom (Oε2) of E^{76} is within hydrogen-bonding distance of W2 (2.6 Å) and is 3.4 Å away from the Ni atom ("carboxylate-out" conformation). The active-site pocket is open and directly accessible from the solvent, thus exposing the water ligands in the active-site

[*] Dr. J.-H. Jeoung, Prof. Dr. H. Dobbek
Institut für Biologie, Strukturbiologie/Biochemie
Humboldt-Universität zu Berlin
Unter den Linden 6, 10099 Berlin (Germany)
E-mail: holger.dobbek@hu-berlin.de
Dr. D. Nianios, Prof. Dr. S. Fetzner
Institut für Molekulare Mikrobiologie und Biotechnologie
Westfälische Wilhelms-Universität Münster
48149 Münster (Germany)

Supporting information and ORCID(s) from the author(s) for this article are available on the WWW under http://dx.doi.org/10.1002/anie.201510741.

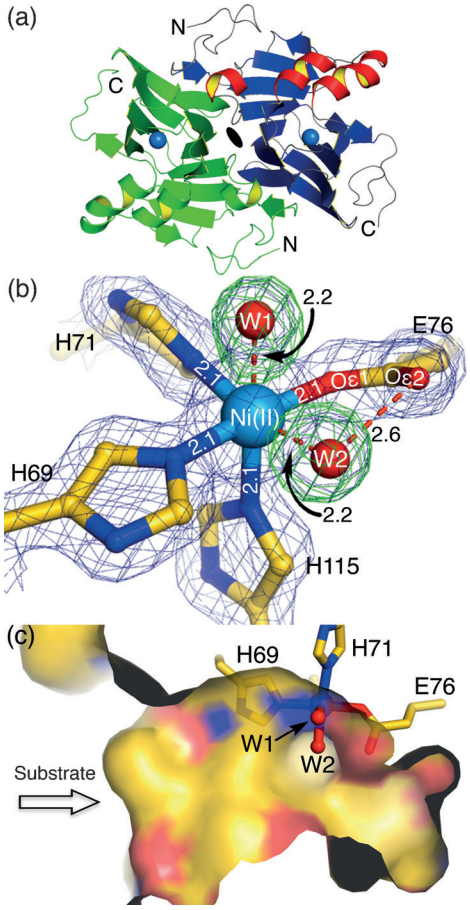

Figure 1. Crystal structure of Ni-QueD in the resting state at 1.80 Å (free E). a) Overall dimeric structure of Ni-QueD. A β-barrel (blue) is shown in one subunit with red α-helices (right molecule) and the second subunit is presented as a green cartoon. The black oval in the middle of the dimer marks a twofold axis. b) Coordination of Ni^{2+} in the resting state. SigmaA-weighted $2F_{obs}-F_{calc}$ (blue mesh) and $F_{obs}-F_{calc}$ omit (green mesh) electron density maps are contoured at 1.5 and 4.0 σ, respectively. Distances in all figures are in Angstrom. c) Surface representation of the active site around the Ni^{2+} ion.

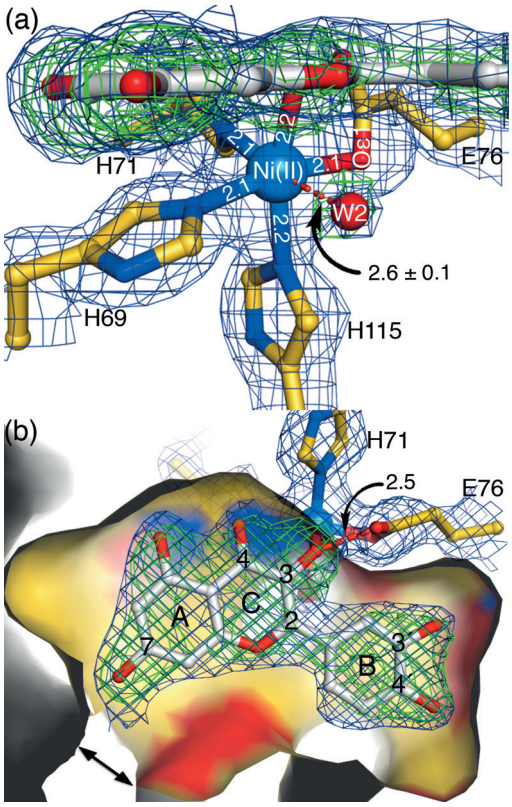

Figure 2. The ES-complex structure at 2.15 Å. a) Binding of QUE to the Ni^{2+} ion. The structure has a similar orientation as in Figure 1b. b) Surface representation of the QUE-bound active site (same orientation as Figure 1c). Carbon atoms of QUE are colored gray, other atoms are colored as in Figure 1. The weighted $2F_{obs}-F_{calc}$ electron density (blue mesh) and $F_{obs}-F_{calc}$ omit difference (green mesh) maps are contoured at 1.2 and 3.5 σ, respectively. The omit map was calculated after excluding QUE and W2.

pocket (Figure 1c). The Ni coordination is similar to that of acireductone dioxygenase.[12] The structure of the 3His-1Glu metal-binding motif is well conserved among QueDs (Figure S5-B–D).[4b,5b]

The crystal structure of Ni-$QueD^{FLA}$ with QUE bound (ES-complex) was determined at a resolution of 2.15 Å (Figure 2 and Table S1). Eleven out of the twelve molecules in the ASU contained QUE, with occupancies of 70–90% and B-factors of approximately 35 $Å^2$ (Table S2). QUE is held in the active-site cavity by three H-bonds and its coordination to nickel (Figure 2 and Figure S1A), and it is surrounded by hydrophobic side chains within van der Waals distance (Figure S1). QUE binds through $O3_{QUE}$ in trans to H^{115} on the nickel ion, replacing a water ligand (W1; Figure 2a). Details of the nickel geometry can be found in Table S3. The carboxylate group of E^{76} rotates approximately 90° upon QUE binding, bringing its Oε2 atom within a short H-bonding distance (2.5 Å) of $O3_{QUE}$, whereby the distance between Oε2 and Ni^{2+} decreases from 3.4 Å to 2.9 Å ("carboxylate-in" conformation). QUE is slightly bent (ca. 5°) at $C2_{QUE}$ and faces outward from the Ni ion (Table S3). While other Ni–ligand bond lengths remain the same, QUE binding weakens the bond between nickel and W2, thereby increasing its length from 2.2 Å to 2.6 ± 0.1 Å ($n = 11$ in ASU).

QUE binding also induces conformational changes in the active-site pocket. QUE binding restrains solvent access to the pocket (Figure 2b) because movements of four hydrophobic residues (F^{36}, P^{67}, F^{165}, and F^{176}), a small helix (lid helix), and E^{64} act as gatekeepers, restricting the narrow entrance (Figure 2b and Figure S1B).

We incubated ES-complex crystals with pure dioxygen for 1–10 min and cryotrapped the reactive state. The resulting crystal structures showed an elongated difference density ($F_{obs}-F_{calc}$ map) at the nickel center, where the water (W2) was bound in the ES-complex (Figure S2). We repeated the same treatment twice and observed similarly elongated densities. When crystals containing the ES-complex were incubated for more than 10 min with dioxygen, the active-site pocket contained little or no electron density for QUE, thus indicating complete turnover and return to the free E state.

Finally, we solved a crystal structure of the ES-complex treated with O_2 at a resolution of 1.82 Å (Table S1). Two out of the twelve chains showed isomorphic elongated positive

densities at the nickel center (chains C and F; Figure 3), whereas the other chains had the same structure as in the ES-complex. When we modelled dioxygen into the elongated electron density, the difference density vanished. In contrast, monoatomic models including a single oxygen atom in this position, such as W2 in the ES-complex, could not explain the difference density, and additional positive density remained next to the modelled water even after several refinement cycles (Figure S3). The model including dioxygen was refined with an occupancy of over 70% and B-factors for the two oxygen atoms of 35 and 36 Å^2 (Table S2).

Dioxygen binds side-on to the Ni^{2+} ion and is perpendicular to the plane of the three rings of QUE. Both Ni–O bond lengths refined to 2.4 Å, thus indicating a weak Ni–O_2 interaction through symmetric side-on binding of O_2 (Figure 3). Owing to the resolution of the structure (d_{min} = 1.82 Å), the $O1_{O2}$–$O2_{O2}$ bond length had to be restrained and can be refined to values between 1.20 and 1.35 Å (see the Supporting Information). $O1_{O2}$ is close to $C2_{QUE}$ (2.6 Å). Binding of O_2 slightly increased the bending angle of QUE at C2 to 7–8° (Figure S4). The remaining coordination environment of the nickel ion does not change upon binding of dioxygen.

Our structures support the following mechanism for substrate activation by Ni-QueD^{FLA} (Figure 4): In the free E state, the nickel in QueD^{FLA} is octahedrally coordinated in an arrangement that includes two water ligands, of which one (W2) is additionally stabilized on the nickel through a short H-bond in the "carboxylate-out" conformation of E^{76} (Figure 4, complex I). Upon forming the ES-complex, the $O3_{QUE}$ group replaces the water ligand (W1) at Ni^{2+} in trans to H^{115} and QUE binds only in a monodentate manner to Ni^{2+} owing to the spatial restraints of the active-site pocket (Figure 4, complex II). Concomitantly, E^{76} changes its conformation to "carboxylate-in" and is now able to deprotonate $HO3_{QUE}$. Binding of QUE together with the associated "carboxylate-in" movement of E^{76} weaken the Ni–water bond, elongating it from 2.2 Å to 2.6 Å (Figure 2a and Figure 4, complex II). This bond-weakening is likely necessary to favour the ligand exchange of W2 against the only weakly binding dioxygen. Concomitant conformational changes not only screen the active site from the solvent but also create a small channel for O_2 diffusion to its binding site at the Ni^{2+} ion (Figure 2b and Figure S1B). Dioxygen entering the active site binds side-on to Ni^{2+} (Figure 3 and Figure 4, complex III).

The electronic state of the Ni:QUE:O_2 complex remains unresolved. Superoxo and peroxo species can be distinguished by their O–O bond lengths. Whereas short O–O bond lengths have been reported for inorganic model complexes with a side-on Ni^{II}-superoxo species (1.35 Å),[13,14] Ni^{III}-peroxo complexes have O–O bond lengths of around 1.4 Å.[15

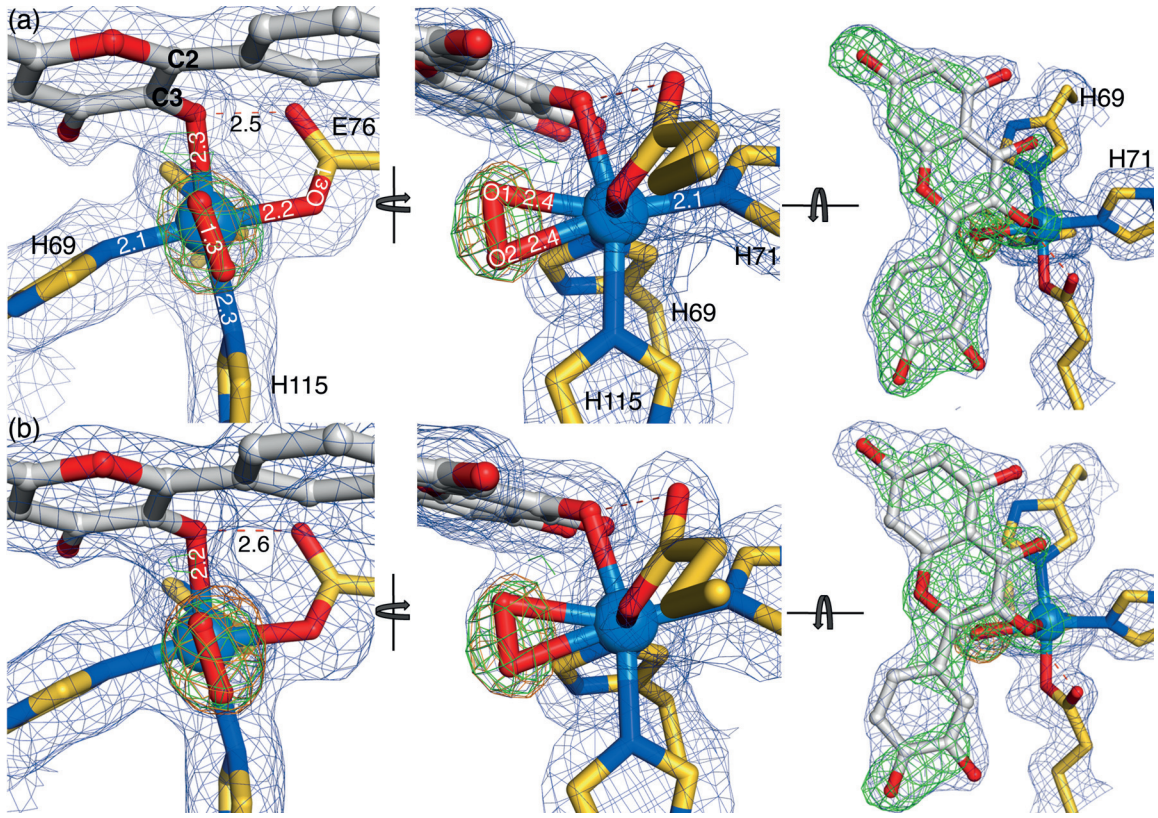

Figure 3. Structure of dioxygen bound to the ES-complex at 1.82 Å (ES:O_2 complex). a, b) ES:O_2 complex structures in chains C and F, respectively. The O1–O2 bond lengths in both chains were refined to 1.30 Å. Only bond lengths differing in both chains are shown in Figure 3b. SigmaA-weighted $2F_{obs}-F_{calc}$ electron density map (blue mesh) is shown with a contour level of 1.5 σ. The weighted $F_{obs}-F_{calc}$ omit difference map in green for QUE and O_2 are contoured at 3.8 σ and calculated after omitting QUE and O_2. A simulated-annealing omit map for dioxygen contoured at 3.6 σ is shown as an orange mesh.

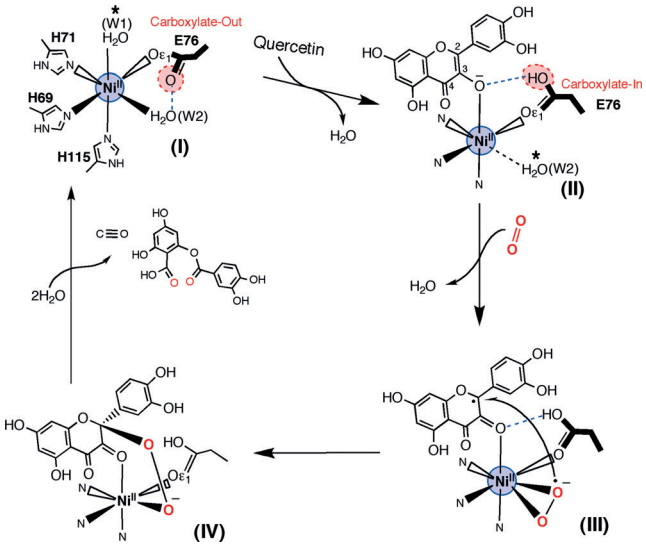

Figure 4. Structure-based reaction mechanism. I) Free E state. II) ES-complex. III) Pre-catalytic ES:O_2 complex. The electron needed to reduce dioxygen to the superoxide anion may either be derived from quercetin (shown) or from Ni^{II}. IV) Peroxydate intermediate before incorporation of two oxygen atoms. Water molecules with a star indicate the site to be replaced by incoming substrates QUE and O_2.

The observed O–O bond length of up to 1.35 Å in the ES:O_2 complex of Ni-QueD^{FLA} would thus account for either dioxygen or superoxide bound to nickel.

After the binding and activation of both substrates, attack of activated O_2 on QUE and cleavage of the O–O and C–C bonds have to occur.[5,16] Based on DFT calculations, Siegbahn et al.[17] suggested that the energetically favoured route starts by forming a C2–O and subsequently C4–O bond before the O–O and two C–C bonds are cleaved simultaneously with liberation of CO and the depside (Figure 4,complex IV). This mechanism is supported by our crystal structures, in which the Ni^{2+}-bound O_2 is close to $C2_{QUE}$ (2.6 Å), which is consistent with a slight overlap of the van der Waals radii of the two atoms and thus requires only minor movements to attain the proposed transition state and initiate the reaction sequence.[17]

In conclusion, Ni^{2+} activates and aligns both substrates for the reaction: QUE by stabilizing its deprotonated, anionic state and O_2 by side-on binding and probably one-electron reduction. Therefore, Ni-QueD^{FLA} reacts like Fe^{2+}-dependent dioxygenases, for example, homoprotocatechuate dioxygenase[18] or homogentisate dioxygenase,[19] and unlike the cofactor-free dioxygenases.[8]

Acknowledgments

The study was supported by the DFG (FE 383/18-1) and EXC 314 "Unifying Concepts of Catalysis - UniCat". We acknowledge access to beamlines of BESSY II (Berlin, Germany) via the Joint Berlin MX-Laboratory.[20] We thank Cornelia Heuberger for support in crystallization, Dr. Stefan Hetz for providing pure dioxygen, and members of our group for discussions.

Keywords: biocatalysis · carbon monoxide · dioxygen activation · dioxygenases · nickel superoxo complexes

How to cite: *Angew. Chem. Int. Ed.* **2016**, *55*, 3281–3284
Angew. Chem. **2016**, *128*, 3339–3343

[1] T. Iwashina, *J. Plant Res.* **2000**, *113*, 287–299.
[2] a) A. M. Marin, E. M. Souza, F. O. Pedrosa, L. M. Souza, G. L. Sassaki, V. A. Baura, M. G. Yates, R. Wassem, R. A. Monteiro, *Microbiology* **2013**, *159*, 167–175; b) S. Tranchimand, P. Brouant, G. Iacazio, *Biodegradation* **2010**, *21*, 833–859.
[3] S. Fetzner, *Appl. Environ. Microbiol.* **2012**, *78*, 2505–2514.
[4] a) F. Fusetti, K. H. Schroter, R. A. Steiner, P. I. van Noort, T. Pijning, H. J. Rozeboom, K. H. Kalk, M. R. Egmond, B. W. Dijkstra, *Structure* **2002**, *10*, 259–268; b) R. A. Steiner, W. Meyer-Klaucke, B. W. Dijkstra, *Biochemistry* **2002**, *41*, 7963–7968; c) B. Gopal, L. L. Madan, S. F. Betz, A. A. Kossiakoff, *Biochemistry* **2005**, *44*, 193–201.
[5] a) D. Buongiorno, G. D. Straganz, *Coord. Chem. Rev.* **2013**, *257*, 541–563; b) R. A. Steiner, K. H. Kalk, B. W. Dijkstra, *Proc. Natl. Acad. Sci. USA* **2002**, *99*, 16625–16630.
[6] A. Nishinaga, T. Tojo, H. Tomita, T. Matsuura, *J. Chem. Soc. Perkin Trans. 1* **1979**, 2511–2516.
[7] a) E. Balogh-Hergovich, G. Speier, *J. Org. Chem.* **2001**, *66*, 7974–7978; b) G. Baráth, J. Kaizer, G. Speier, L. Párkányi, E. Kuzmann, A. Vértes, *Chem. Commun.* **2009**, 3630–3632; c) Y. J. Sun, Q. Q. Huang, J. J. Zhang, *Dalton Trans.* **2014**, *43*, 6480–6489.
[8] a) R. A. Steiner, H. J. Janssen, P. Roversi, A. J. Oakley, S. Fetzner, *Proc. Natl. Acad. Sci. USA* **2010**, *107*, 657–662; b) S. Fetzner, *Nat. Chem. Biol.* **2007**, *3*, 374–375; c) S. Thierbach, N. Bui, J. Zapp, S. R. Chhabra, R. Kappl, S. Fetzner, *Chem. Biol.* **2014**, *21*, 217–225.
[9] a) H. Merkens, S. Sielker, K. Rose, S. Fetzner, *Arch. Microbiol.* **2007**, *187*, 475–487; b) H. Merkens, R. Kappl, R. P. Jakob, F. X. Schmid, S. Fetzner, *Biochemistry* **2008**, *47*, 12185–12196.
[10] D. Nianios, S. Thierbach, L. Steimer, P. Lulchev, D. Klostermeier, S. Fetzner, *BMC Biochem.* **2015**, *16*, 1–10.
[11] L. Rulíšek, J. Vondrášek, *J. Inorg. Biochem.* **1998**, *71*, 115–127.
[12] "Nickel in Acireductone Dioxygenase": T. C. Pochapsky, T. Ju, M. Dang, R. Beaulieu, G. M. Pagani, B. OuYang, in *Nickel and Its Surprising Impact in Nature*, *Vol. 2* (Eds.: A. Sigel, H. Sigel, R. K. O. Sigel), Wiley, Chichester, **2007**.
[13] a) C. J. Cramer, W. B. Tolman, K. H. Theopold, A. L. Rheingold, *Proc. Natl. Acad. Sci. USA* **2003**, *100*, 3635–3640; b) P. L. Holland, *Dalton Trans.* **2010**, *39*, 5415–5425.
[14] a) S. Yao, E. Bill, C. Milsmann, K. Wieghardt, M. Driess, *Angew. Chem. Int. Ed.* **2008**, *47*, 7110–7113; *Angew. Chem.* **2008**, *120*, 7218–7221; b) K. Fujita, R. Schenker, W. W. Gu, T. C. Brunold, S. P. Cramer, C. G. Riordan, *Inorg. Chem.* **2004**, *43*, 3324–3326.
[15] a) J. Cho, R. Sarangi, W. Nam, *Acc. Chem. Res.* **2012**, *45*, 1321–1330; b) J. Cho, H. Y. Kang, L. V. Liu, R. Sarangi, E. I. Solomon, W. Nam, *Chem. Sci.* **2013**, *4*, 1502–1508.
[16] G. D. Straganz, B. Nidetzky, *ChemBioChem* **2006**, *7*, 1536–1548.
[17] P. E. M. Siegbahn, *Inorg. Chem.* **2004**, *43*, 5944–5953.
[18] E. G. Kovaleva, J. D. Lipscomb, *Science* **2007**, *316*, 453–457.
[19] J.-H. Jeoung, M. Bommer, T. Y. Lin, H. Dobbek, *Proc. Natl. Acad. Sci. USA* **2013**, *110*, 12625–12630.
[20] U. Mueller, N. Darowski, M. R. Fuchs, R. Forster, M. Hellmig, K. S. Paithankar, S. Puhringer, M. Steffien, G. Zocher, M. S. Weiss, *J. Synchrotron Radiat.* **2012**, *19*, 442–449.

Received: November 19, 2015
Published online: February 5, 2016

